LLNL-JRNL-716017

Direct Metal Writing: Controlling the Rheology through Microstructure

W. Chen, L. Thornley, H. G. Coe, E. B. Duoss, R. Hunt, M. Wight, D. Apelian, A. J. Pascall, J. D. Kuntz, C. M. Spadaccini, S. J. Tonneslan, J. J. Vericella, C. Zhu

December 21, 2016

Applied Physics Letters

Direct Metal Writing: Controlling the Rheology through Microstructure

Wen Chen [1,a)], Luke Thornley [2], Hannah G. Coe [1], Samuel J. Tonneslan [2], John J. Vericella [1], Cheng Zhu [1], Eric B. Duoss [1], Ryan M. Hunt [1], Michael J. Wight [3], Diran Apelian [3], Andrew J. Pascall [1,a)], Joshua D. Kuntz [2,a)], Christopher M. Spadaccini [1,a)]

1. Engineering Directorate, Lawrence Livermore National Laboratory, 7000 East Ave, Livermore, CA, 94550, USA

2. Physical and Life Sciences Directorate, Lawrence Livermore National Laboratory, 7000 East Ave, Livermore, CA, 94550, USA

3. Department of Mechanical Engineering, Worcester Polytechnic Institute, Worcester, MA, 01609, USA.

Abstract

Most metal additive manufacturing approaches are based on powder-bed melting techniques such as laser selective melting or electron beam melting, which often yield uncontrolled microstructures with defects (e.g., pores or microcracks) and residual stresses. Here, we introduce a proof-of-concept prototype of a 3D metal freeform fabrication process by direct writing of metallic alloys in the semi-solid regime. This process is achieved through controlling the particular microstructure and the rheological behavior of semi-solid alloy slurries which demonstrate a well suited viscosity and shear thinning property to retain shape upon printing. The ability to control microstructure through this method yields a flexible manufacturing route to fabricating 3D metal parts with full density and complex geometries.

[a]) Authors to whom correspondence should be addressed. Electronic addresses: chen91@llnl.gov (W. Chen); apascall@llnl.gov (A. Pascall); kuntz2@llnl.gov (J. Kuntz); spadaccini2@llnl.gov (C. Spadaccini), Tel.: 01-925-423-3185.

Additive manufacturing (AM) or 3D printing is a process of creating parts by depositing and joining materials layer by layer from 3D models.[1-2] The capability of freeform fabrication of 3D complex objects without the need for expensive tooling or machining has made AM promising for a wide variety of applications. Over the past decades, various AM techniques have been developed to fabricate complex architectures with engineered mechanical or functional properties. For example, projection microstereolithography has been introduced to achieve ultra-light micro-lattices which demonstrate unprecedented specific strength and stiffness.[3-5] Direct ink writing has enabled fabrication of many functional materials and structures such as biological implants and architectures,[6-8] photonic crystals,[9,10] batteries,[11] foldable origami lattices,[12] eutectic salts,[13] and supercapacitors.[14] Fused deposition modeling has been well explored and commercialized in making polymeric structures by melting and extruding thermoplastics (e.g., polycarbonate, acrylonitrile butadiene styrene) in a solid filamentary form.[15,16] However, these AM technologies are often developed for non-metallic materials and are not well-suited for direct printing of metals. Although metal components play an overwhelming role in many industries (e.g., aerospace, medical, and automotive), AM of metals remains challenging. Technologies for metal AM primarily include laser selective melting,[17-19] laser selective sintering,[20,21] laser engineered net-shaping,[22] rheocasting based forming or printing,[23-25] molten metal jetting, [26,27] electron beam melting, [28-30] and electron beam wire welding.[31] Whereas rheocasting based printing has been attempted for metal AM, complex architectures with overhanging features has been proven difficult by this method.[23-25] Most of other metal AM processes rely on metal powder-based melting techniques which have some inherent limitations. For example, powder melting is typically associated with complex thermal histories, which often bring residual stresses, micro-cracks, and uncontrolled microstructures within the fabricated parts.[32] The progressive melting and binding of metal powders can also lead to non-fully dense parts where porosity has been an issue.[18] The existence of these microstructural defects often necessitate some post-processing such as hot isostatic pressing or heat treatment to improve the mechanical performance of the resultant parts.[33,34] Such post-processing and the low deposition rate by powder-based metal AM also impose a high manufacturing cost.

In this letter, we introduce an alternative low cost approach for AM of metal alloys. This method is based on direct metal writing (DMW) of metallic alloys in the semi-solid state through controlling the particular microstructure and the rheological behavior of semi-solid alloy slurries. Here, semi-solid slurries refer to metallic melts of solid-liquid mixtures in the region between solidus and liquidus lines in the equilibrium phase diagram. The unique viscosity and shear thinning characteristic of the semi-solid alloys allows readily controlled geometries during steady state printing. In addition, the high versatility in maneuvering the microstructural features during solidification of the semi-solid slurries suggests a flexible AM route to fabricating 3D metal parts with full density and designed properties that may be inaccessible by conventional metal AM or other processing methods. To demonstrate the fundamental principle of this approach, we will show a proof-of-concept DMW prototype of a simple and low temperature Bi-Sn binary semi-solid alloy system as a representative example. Due to the comparable melting temperature and flow properties to conventional Sn-Pb solder alloy, Bi-Sn alloys have been identified as a class of promising lead-free solder alloy system, [35,36] and the ability to print these alloys will also offer insight into many applications such as printed electronic interconnects and electronic circuit architecture assembly.

Alloy rod-shaped ingots of 15 mm diameter with nominal composition of $Bi_{75}Sn_{25}$ (at.%) was purchased from Sophisticated Alloys Inc. The ingots were generated by arc-melting and casting high purity (> 99.99%) raw elements under an argon atmosphere. The solidus temperature (T_s) and the liquidus temperature (T_l) of the alloy ingots were identified by differential scanning calorimetry (DSC) to be 139 ºC and 225 ºC at a heating rate of 10 ºC/min, respectively, which are comparable to the data from the equilibrium Bi-Sn phase diagram (Supplementary Material Fig. S1). The alloy ingots were cut into pieces and fed into the DMW system, which is composed of a reservoir with an extended nozzle, a nitrogen pressure source, and a printing substrate (Fig. 1). Resistance heaters with attached PID controlled thermocouples were used to heat the semi-solid alloy with a precision of ± 2 ºC. In this study, DMW relies on the rheological properties that are mechanistically determined by the microstructure of the semi-solid alloys. Previous studies on semi-solid alloy processing (e.g., rheocasting or thixoforming) have revealed that temperature and external shearing are two important factors that can be manipulated to effectively tailor the microstructure, the rheological characteristics, and the formability of semi-solid alloys.[37-41] Microscopically, processing temperature determines the volume fraction of the solid phase. External shearing tends to break large dendrites and thereby significantly affects the morphology of the dispersed solid phases within the semi-solid alloys. To apply shear force to the semi-solid alloy during DMW, a motor driven grooved spindle was inserted in the center of the nozzle (Fig. 1). For the purpose of understanding the rheological flow of $Bi_{75}Sn_{25}$ and exploiting appropriate protocols for DMW of $Bi_{75}Sn_{25}$, a systematic study of the rheological behavior of $Bi_{75}Sn_{25}$ at different temperatures (T) and different shear rates ($\dot{\gamma}$) was performed using an oscillatory rheometer (Anton Paar MCR 502 with a CTD-1000 attachment, profiled graphite CC24 measurement Mooney-Ewart geometry, see Supplementary Materials for rheological test details). Akin to many classes of colloidal inks that were developed for direct ink writing,[42-44] we found that the apparent viscosity (η) of $Bi_{75}Sn_{25}$ semi-solid alloy is highly dependent on the temperature and the shear rate (Fig. 2a). η systematically decreases with increasing temperature that is associated with a lower volume fraction (v_f) of the solid primary phase in the slurry. When $\dot{\gamma} = 10\ \mathrm{s}^{-1}$, for example, η dramatically decreases by three orders of magnitude from ~ 4×10^4 mPa•s at T = 190 ºC to ~ 40 mPa•s at T = 210 ºC (Fig. 2a), accompanied by a significant decrease in volume fraction of the solid phase from approximately 32.7% to 14.2% (estimated from the equilibrium phase diagram, Fig. S1). In addition to such a non-Newtonian shear thinning behavior, the $Bi_{75}Sn_{25}$ semi-solid slurry exhibits a strong viscoelastic characteristic within the semi-solid regime (Fig. 2b). Specifically, the storage modulus (G') and the loss modulus (G'') are sensitive to varying shear stresses (or strains) and form a "crossover", which yields a more liquid-like behavior ($G'' > G'$) under large shear stresses and a more solid-like "yielding" behavior ($G'' < G'$) under lower shear stresses (Fig. 2b). The shear thinning and the viscoelastic behaviors are necessary to facilitate the extrusion flow under pressure and the rapid pseudoplastic-to-dilatant recovery to allow shape retention after DMW deposition.

Based on the above rheological parameters, DMW of $Bi_{75}Sn_{25}$ was carried out in the semi-solid regime using a 1 mm diameter nozzle robotically positioned by a three-axis motion stage. $Bi_{75}Sn_{25}$ metallic structures were printed onto a high temperature masking tape covered steel substrate with an optional heater mounted on the underside. The nozzle-to-substrate distance was kept approximately 0.7 mm to ensure moderate adhesion of the as-deposited filament to the substrate and between adjacent printed layers. As the metal slurry exits the nozzle, solidification rapidly occurs, which results in formation of a continuous filament retaining a rod-like shape (Fig. 3a). A representative movie of the filament extrusion process is demonstrated in the Supplementary Material. The marked shear thinning behavior and the rapid solidification of the semi-solid slurry collectively enable fabrication of 3D overhanging structures where filament can span over a wide unsupported region (Fig. 3b). In order to maintain a precise printed feature size, the solidification rate should be comparable to the extrusion rate. Hence, a linear printing speed in the range of 1~10 mm/s is used to accommodate with other solidification rate related processing parameters such as the applied pressure, the printing temperature, shear rate, and the nozzle to substrate distance. This linear printing speed is approximately an order of magnitude lower than typical printing speed by laser selective melting.[45,46] For steady state DMW, a varied nitrogen pressure (P) up to 0.6 MPa was applied into the reservoir to accommodate the different viscosities at varying printing temperatures and shear rates at a typical printing speed of 5 mm/s. For example, the two representative cases of DMW printed $Bi_{75}Sn_{25}$ structures were achieved under two different processing conditions. The "zigzag" shaped pattern (Fig. 3a) was printed at T = 200 ºC, $v_f \approx 27.5\%$, and a spindle speed of ω = 50 rpm was applied to attain a shear rate of $\dot{\gamma} = 50\ \mathrm{s}^{-1}$ ($\dot{\gamma} \approx \frac{2\omega r_2^{\,2}}{(r_2^{\,2}-r_1^{\,2})}$, r_1: spindle radius, r_2: nozzle radius), which gives rise to $\eta \approx 0.1$ Pa•s. An extrusion pressure of P = 0.21 MPa (30 psi) was applied to achieve steady state deposition. In contrast, the two layered lattice (Fig. 3b) was printed at T = 190 ºC, $v_f \approx 32.7\%$, $\dot{\gamma} = 100\ \mathrm{s}^{-1}$, $\eta \approx$ 4 Pa•s, and P = 0.48 MPa (70 psi). The required extrusion pressure to drive the steady state flow of the semi-solid slurry through the nozzle is governed by the shear flow resistance and the frictional resistance against the reservoir and nozzle walls. Hence, the extrusion pressure can be theoretically estimated by a plane strain extrusion model: [47]

$$P \approx \sigma_s\left(\frac{1+c}{c}\right)\left(\frac{W^2}{D^2} - 1\right)^c \qquad (1)$$

if we assume the shear resistance of the semi-solid alloy is rate-independent for low strain rate extrusion (low printing speeds). Here, σ_s denotes the shear strength of the semi-solid alloy and is on the order of $10 \sim 10^2$ kPa for the considered viscosity range;[37] $c = f/tan\alpha$ is the nozzle geometry related frictional coefficient, where $f \approx 0.1$ the empirical friction coefficient [48] and $\alpha \approx 30^{o}$ the tapered angle of the nozzle; $D = 1$ mm and $W = 14$ mm are the nozzle tip diameter and the reservoir outer diameter, respectively. Therefore, a required pressure range of $P \approx 0.17 \sim 1.7$ MPa is quantitatively predicted to allow extrusion under the above DMW conditions for $Bi_{75}Sn_{25}$. This is comparable to the experimentally applied pressure range for the two representative DMW protocols. It should be noted that from Eq. (1), a decrease in nozzle size (D) can dramatically increase the pressure demand for DMW, and it is thereby difficult to utilize nozzles with $D < 1$ mm at a practical pressure range in this study.

In general, the property of a material is fundamentally linked to its microstructure. To identify the internal microstructures of printed $Bi_{75}Sn_{25}$ semi-solid alloy, the cross-sections of the filaments from the two representative prints were carefully polished and examined by scanning electron microscopy (SEM) equipped with energy dispersive spectroscopy (EDS). The microstructure of both filaments is comprised of two contrasting phases, the $30 \sim 50$ μm polygonal primary Bi blocks and the Bi-Sn eutectic matrix (Fig. 3c and Fig. 3d). The polygonal block-like geometry of the uniformly dispersed primary Bi phase revealed herein is tremendously different from the typical needle-like dendrite geometry in most Bi-Sn alloys.[49] This can be understood from the perspective of applied shearing during DMW that gives rise to the fragmentation of large or long needle-like Bi dendrites and prevents nozzle clogging upon printing. For comparison, the microstructure of a $Bi_{75}Sn_{25}$ filament printed at 200 ºC without shear is shown in Fig. 3e, where many long needle-like Bi dendrites emerge, clog the nozzle, and prevent steady state printing. It is worth noting that the microstructural morphology of the two representative steady state DMW prints is also slightly different (Fig. 3c and 3d). Specifically, compared to the microstructure of the "zigzag" filament, we found a higher volume fraction of finer Bi-rich precipitates in the as-printed filament of the two layered lattice. This is attributed to a higher shear rate and a higher volume fraction of pre-existing Bi solid phase within the slurry at a lower printing temperature for the two layered lattice. Such different microstructures suggest that DMW provides a powerful toolbox to create parts with facilely controlled microstructures by employing a wide range of DMW processing protocols. In this aspect, DMW is a more predictive AM method in microstructural control than many other metal AM approaches such as selective laser melting or electron beam melting. However, specific attention should be paid to the long-term crystal growth within the equilibrium semi-solid alloys, even under an external shear stress.[38] Hence, a sluggish crystal growth kinetic of the precipitate in the semi-solid alloy system is desired to achieve long-term steady state printing of alloys with a highly controlled microstructure.

In addition to the microstructure of the filament, we also investigated the microstructure of the interfacial joint between adjacent layers. Interestingly, we found a smooth and continuous interfacial transition with no distinguishable defects when the printing substrate was heated at 100 ºC during DMW (Fig. 4a) whereas a discontinuous interface with micro-cracks was detected when the substrate was not heated (Fig. 4b). The interfacial bonding between adjacent layers depends on the temperature difference and heat transfer between the semi-solid slurry and the as-printed underlying layer. To interpret and quantify the underlying mechanism of the joining process, a criterion for forming a reliable metallurgical bond is introduced based on an interfacial heat transfer model. For simplicity, we assume a one-dimensional heat transfer process across the interface and a constant interfacial temperature without convective cooling. A thermal energy balance at the interface requires the heat loss by the slurry to be equal to the heat absorbed by the underlying layer,[50] i.e.,

$$\rho_1\, c_{p1}(T_1 - T_i)^2 = \rho_2\, c_{p2}(T_i - T_2)^2 \qquad (2)$$

where ρ_1, ρ_2 the density, T_1, T_2 the temperature, c_{p1}, c_{p2} the specific heat capacity of the slurry and the underlying layer, respectively. T_i is the interfacial temperature at the moment of interfacial contact. To establish a strong metallurgical bond at the interface, the interface should be re-melted into the semi-solid regime. It is however difficult to clearly define the minimum T_i that is required to activate the interfacial re-melting and flow. For simplicity, we assume that the solidus temperature sets the minimum T_i (i.e., T_i = T_s) although this may cause some underestimation. For $Bi_{75}Sn_{25}$ alloy, $T_i \approx 139$ ºC. c_p of metallic alloys are generally temperature dependent. $c_p \approx 0.6$ $J/g{\cdot}K$ and $\approx$ 0.16 $J/g{\cdot}K$ for $Bi_{75}Sn_{25}$ within the semi-solid regime and the pure solid regime, respectively (e.g., we measured $c_p \approx 0.58$ $J/g{\cdot}K$ and 0.15 $J/g{\cdot}K$ at 190 ºC, and 50 ºC, respectively, see Supplementary Material Fig. S1). This indicates that for typical printing of semi-solid $Bi_{75}Sn_{25}$, pre-heating of the printing substrate is needed to ensure reliable interfacial bonding. For example, a minimum under-layer substrate temperature of $T_2 \approx 40$ ºC is required to print well-bonded structures at a printing temperature of 190 ºC. Note that this is the lower bound approximation by assuming T_i = T_s and neglecting additional thermal energy loss due to convective cooling.

In summary, we introduce an alternative approach to additive manufacturing of metals by DMW of semi-solid alloys. Our approach is realized through controlling the microstructure of semi-solid alloy slurries to access an appropriate rheological behavior, particularly a well-suited viscosity range and a shear thinning characteristic, which allow steady state printing of 3D metallic structures. A facile control of the microstructural features during solidification can be mediated via manipulating the DMW protocols. The inherent flexibility of DMW over conventional metal AM processes opens up a yet unexplored avenue for metal AM and offers the potential to pursue a myriad of applications for metals. The ability to print $Bi_{75}Sn_{25}$ alloy offers insight into applications such as printed electronic interconnects. The principle of the DMW printed $Bi_{75}Sn_{25}$ prototype described in this study can be universally extended to a vast range of other semi-solid alloys which possess a reasonable semi-solid region. DMW of technically more interesting alloy systems such as Al alloys (e.g., A356), Mg alloys, Ti alloys and steels will be a key subject of future work.

Supplementary Material

Please see Supplementary Material for Bi-Sn binary phase diagram, thermal characteristics, and the rheology test details of $Bi_{75}Sn_{25}$ alloy.

This work was financially supported by Laboratory Directed Research and Development 14-SI-004. This work was performed under the auspices of the U.S. Department of Energy by Lawrence Livermore National Laboratory under Contract DE-AC52-07NA27344. We are very grateful for the experimental assistance from Scott E. Fisher, Tianyi Kou, and Dr. Sungwoo Sohn. LLNL-JRNL-716017.

References

[1] K.V. Wong and A. Hernandez, ISRN Mechanical Engineering, 2012 (2012).

[2] J.J. Beaman, J.W. Barlow, D.L. Bourell, R.H. Crawford, H.L. Marcus, and K.P. McAlea, *Solid freeform fabrication: a new direction in manufacturing*, Kluwer Academic Publishers, Norwell, MA, **2061**, 25 (1997).

[3] T.A. Schaedler, A.J. Jacobsen, A. Torrents, A.E. Sorensen, J. Lian, J.R. Greer, L. Valdevit, and W.B. Carter, Science, **334**, 962 (2011).

[4] X. Zheng, H. Lee, T.H. Weisgraber, M. Shusteff, J. DeOtte, E.B. Duoss, J.D. Kuntz, M.M. Biener, Q. Ge, J.A. Jackson, S.O. Kucheyev, N.X. Fang, and C.M. Spadaccini, Science, **344**, 1373 (2014).

[5] A. Torrents, T. Schaedler, A. Jacobsen, W. Carter, and L. Valdevit, Acta Mater. **60,** 3511 (2012).

[6] N.G. Durmus, S. Tasoglu and U. Demirci, Nat. Mater. **12**, 478 (2013).

[7] J.N. Hanson Shepherd, S.T. Parker, R.F. Shepherd, M.U. Gillette, J.A. Lewis, and R.G. Nuzzo, Adv. Funct. Mater. **21**, 47 (2011).

[8] A.E. Jakus, S.L. Taylor, N.R. Geisendorfer, D.C. Dunand, and R.N. Shah, Adv. Funct. Mater. **25**, 6985 (2015).

[9] E.B. Duoss, M. Twardowski, and J.A. Lewis, Adv. Mater. **19**, 3485 (2007).

[10] F. García-Santamaría, M. Xu, V. Lousse, S. Fan, P.V. Braun, and J.A. Lewis, Adv. Mater. **19**, 1567 (2007).

[11] K. Sun, T.S. Wei, B.Y. Ahn, J.Y. Seo, S.J. Dillon, and J.A. Lewis, Adv. Mater. **25**, 4539 (2013).

[12] B.Y. Ahn, D. Shoji, C.J. Hansen, E. Hong, D.C. Dunand, and J.A. Lewis, Adv. Mater. **22**, 2251 (2010).

[13] J.W. Boley, K. Chaudhary, T.J. Ober, M. Khorasaninejad, W.T. Chen, E. Hanson, A. Kulkarni, J. Oh, J. Kim, L.K. Aagesen, A.Y. Zhu, F. Capasso, K. Thornton, P.V. Braun, and J.A. Lewis, Adv. Mater. **1604778** (2016).

[14] C. Zhu, T. Liu, F. Qian, T.Y.-J. Han, E.B. Duoss, J.D. Kuntz, C.M. Spadaccini, M.A. Worsley, and Y. Li, Nano Lett. **16**, 3448 (2016).

[15] H. Ramanath, C. Chua, K. Leong, and K. Shah, J. Mater Sci. Mater in Medicine, **19**, 2541 (2008).

[16] D. Bourell, B. Stucker, R. Ilardo, and C.B. Williams, Rapid Prototyping J, **16**, 174 (2010).

[17] J.-P. Kruth, L. Froyen, J. Van Vaerenbergh, P. Mercelis, M. Rombouts, and B. Lauwers, J. Mater. Process Tech. **149**, 616 (2004).

[18] J.-P. Kruth, P. Mercelis, J. Van Vaerenbergh, L. Froyen, and M. Rombouts, Rapid Prototyping J, **11**, 26 (2005).

[19] M. Seifi, A. Salem, J. Beuth, O. Harrysson, and J.J. Lewandowski, JOM, **68**, 747 (2016).

[20] M. Agarwala, D. Bourell, J. Beaman, H. Marcus, and J. Barlow, Rapid Prototyping J, **1**, 26 (1995).

[21] S. Das, M. Wohlert, J.J. Beaman, and D.L. Bourell, JOM, **50**, 17 (1998).

[22] W. Hofmeister, M. Wert, J. Smugeresky, J.A. Philliber, M. Griffith, and M. Ensz, JOM **51**, 1 (1999).

[23] C.S. Rice, P.F. Mendez, and S.B. Brown, JOM, **52**, 31 (2000).

[24] G. Hirt, L. Khizhnyakova, R. Baadjou, F. Knauf, and R. Kopp, *Thixoforming: semi-solid metal processing*, 1 (2009).

[25] S. Finke and F. Feenstra, J. Mater. Sci., **37**, 3101 (2002).

[26] J.W. Priest, C. Smith, and P. DuBois, in: *Solid Freeform Fabrication Proceedings, University of Texas at Austin, TX*, 1997, pp. 1-10.

[27] K. Yamaguchi, K. Sakai, T. Yamanaka, and T. Hirayama, Prec. Eng., **24**, 2 (2000).

[28] L.E. Murr, S.M. Gaytan, D.A. Ramirez, E. Martinez, J. Hernandez, K.N. Amato, P.W. Shindo, F.R. Medina, and R.B. Wicker, J. Mater. Sci. Technol. **28**, 1 (2012).

[29] E. Hernández-Nava, C. Smith, F. Derguti, S. Tammas-Williams, F. Leonard, P. Withers, I. Todd, and R. Goodall, Acta Mater. **108**, 279 (2016).

[30] C. Smith, F. Derguti, E.H. Nava, M. Thomas, S. Tammas-Williams, S. Gulizia, D. Fraser, I. Todd, J. Mater. Process Tech. **229**, 128 (2016).

[31] W.E. Frazier, J. Mater. Eng Perform. **23**, 1917 (2014).

[32] D. Gu, Y.-C. Hagedorn, W. Meiners, G. Meng, R.J.S. Batista, K. Wissenbach, and R. Poprawe, Acta Mater. **60**, 3849 (2012).

[33] B. Vrancken, L. Thijs, J.-P. Kruth, and J. Van Humbeeck, J. Alloys. Compd. **541**, 177 (2012).

[34] S. Leuders, M. Thöne, A. Riemer, T. Niendorf, T. Tröster, H. Richard, and H. Maier, Int. J. Fatigue **48**, 300 (2013).

[35] W.R. Osório, L.C. Peixoto, L.R. Garcia, N. Mangelinck-Noël, and A. Garcia, J. Alloys Compd. **572**, 97 (2013).

[36] M. Abtew and G. Selvaduray, Mater. Sci. Eng. R **27**, 95 (2000).

[37] M.C. Flemings, Metall. Trans. B, **22**, 269 (1991).

[38] J. Koke and M. Modigell, J. Non-Newtonian Fluid **112**, 41 (2003).

[39] O. Lashkari and R. Ghomashchi, J. Mater. Process Tech. **182**, 229 (2007).

[40] D. Apelian, Y. Tsutsui, M. Kiuchi, and K. Ichikawa, in: TSUTSUI Y, KIUCHI M, ICHIKAWA K. Proc of the 7th Int Conf on the Processing of Semi-Solid Alloys and Composite. Tsukuba, Japan, 2002, pp. 25-30.

[41] Q. Pan, D. Apelian, and A. Alexandrou, Metall. Mater. Trans. B **35**, 1187 (2004).

[42] E.B. Duoss, T.H. Weisgraber, K. Hearon, C. Zhu, W. Small, T.R. Metz, J.J. Vericella, H.D. Barth, J.D. Kuntz, R.S. Maxwell, C.M. Spadaccini, and T.S. Wilson, Adv. Funct. Mater. **24**, 4905 (2014).

[43] K.T. Sullivan, C. Zhu, E.B. Duoss, A.E. Gash, D.B. Kolesky, J.D. Kuntz, J.A. Lewis, and C.M. Spadaccini, Adv. Mater. **28**, 1934 (2016).

[44] C. Zhu, T.Y.-J. Han, E.B. Duoss, A.M. Golobic, J.D. Kuntz, C.M. Spadaccini, and M.A. Worsley, Nat. Comm. 6 (2015).

[45] W.E. Frazier, J. Mater. Eng. Perform 23, 1917 (2014).

[46] M. Malinauskas, A. Žukauskas, S. Hasegawa, Y. Hayasaki, V. Mizeikis, R. Buividas and S. Juodkazis, Light: Science & Applications (2016) 5, e16133; doi:10.1038/lsa.2016.133.

[47] O. Hoffman and G. Sachs, *Introduction to the Theory of Plasticity for Engineers*, McGraw-Hill, 1953.

[48] D.H. Kirkwood, M. Suéry, P. Kapranos, H.V. Atkinson, and K.P. Young, *Semi-solid processing of alloys*, Springer, 2010.

[49] W. Chen, J. Kong, and W. Chen, J. Min. Metall. B: Metall. **47**, 11 (2011).

[50] W.M. Rohsenow, J.P. Hartnett, and E.N. Ganic, *Handbook of heat transfer fundamentals*, New York, McGraw-Hill Book Co., 1985.

Figure Captions

FIG. 1 (a) Schematic diagram and (b) real image of the DMW system, which is comprised of an upper reservoir with an extended nozzle and a bottom printing substrate. A motor driven grooved spindle was inserted in the center of the nozzle to apply shear force to the semi-solid alloy.

FIG. 2 Rheological properties of the $Bi_{75}Sn_{25}$ semi-solid alloy slurry. (a) Shear rate dependence of the apparent viscosity at different temperatures; (b) shear strain dependence of storage modulus (*G'*) and loss modulus (*G''*) for considered $Bi_{75}Sn_{25}$ alloy in the semi-solid regime at a representative temperature of T = 200 ºC. The cross-over of *G'* and *G''* with varying shear strain of the semi-solid alloy is necessary for printability, suggesting a liquid-like behavior during DMW whereas a solid-like behavior after printing to facilitate shape retention.

FIG. 3 DMW fabricated $Bi_{75}Sn_{25}$ structures and their microstructures. The characteristic feature size of the filament is close to the nozzle size. (a) "zigzag" pattern printed at 200 ºC; (b) two layered lattice structure with overhanging features (blue inset) printed at 190 ºC; (c) and (d) filament microstructures of prints (a) and (b), respectively, exhibiting a mixture of polygonal Bi blocks and the Bi-Sn eutectic matrix; (e) a $Bi_{75}Sn_{25}$ filament printed at 200 ºC without shear. Many long need-like dendrites tend to clog the nozzle and hence prevent steady state printing.

FIG. 4 (a) Reliable metallurgical bond with a smooth transition at the interface as the printing substrate is heated to 100 ºC for DMW of $Bi_{75}Sn_{25}$ at 190 ºC; (b) inadequate interfacial bond with many visible defects at the interface as the printing substrate is not heated for DMW of $Bi_{75}Sn_{25}$ at 190 ºC.

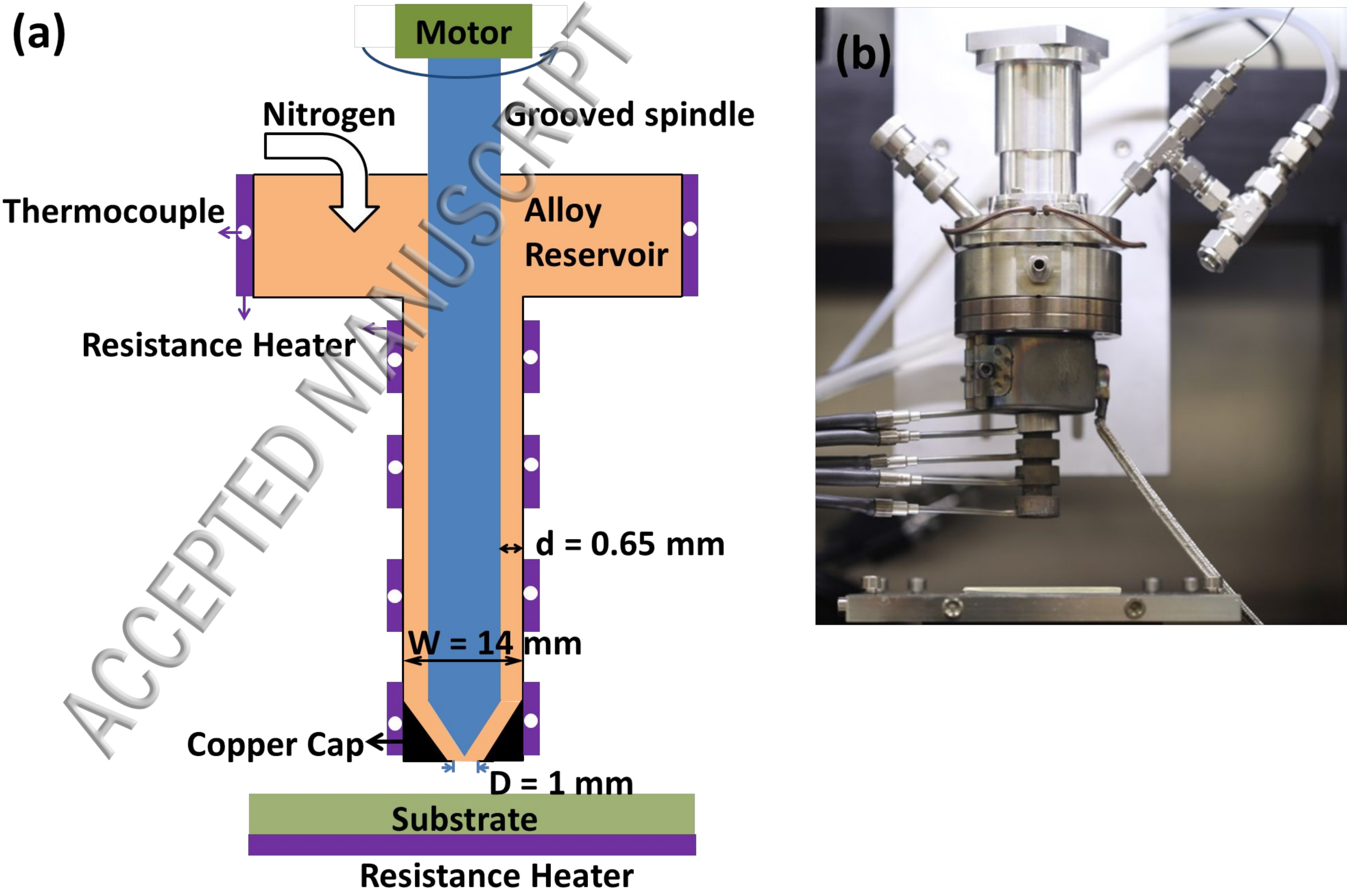
(a)
Motor
Nitrogen
Grooved spindle
Thermocouple
Alloy
Reservoir
Resistance Heater
d = 0.65 mm
W = 14 mm
Copper Cap
D = 1 mm
Substrate
Resistance Heater
(b)

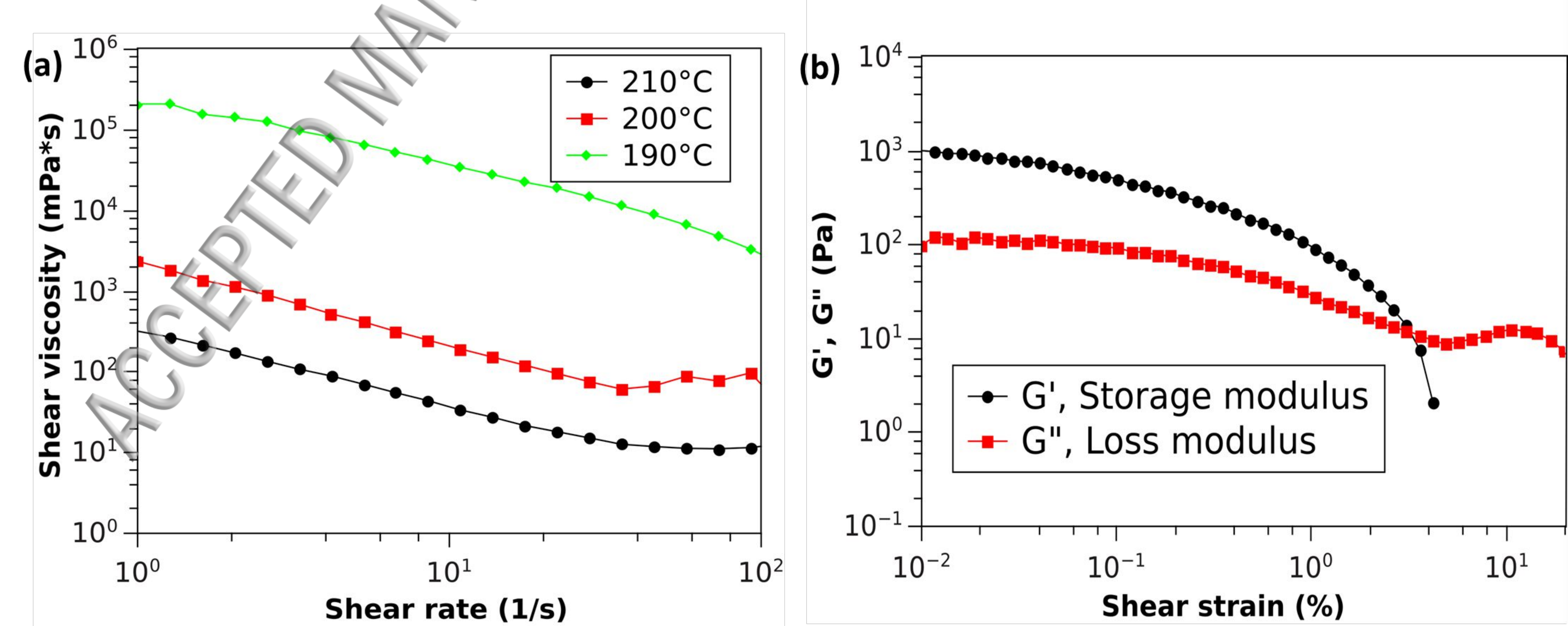
(a)
Shear viscosity (mPa*s)
Shear rate (1/s)
210°C
200°C
190°C
10^{0}
10^{1}
10^{2}
10^{3}
10^{4}
10^{5}
10^{6}
(b)
G', G" (Pa)
Shear strain (%)
G', Storage modulus
G", Loss modulus
10^{-1}
10^{-2}
10^{-1}
10^{0}
10^{1}
10^{2}
10^{3}
10^{4}

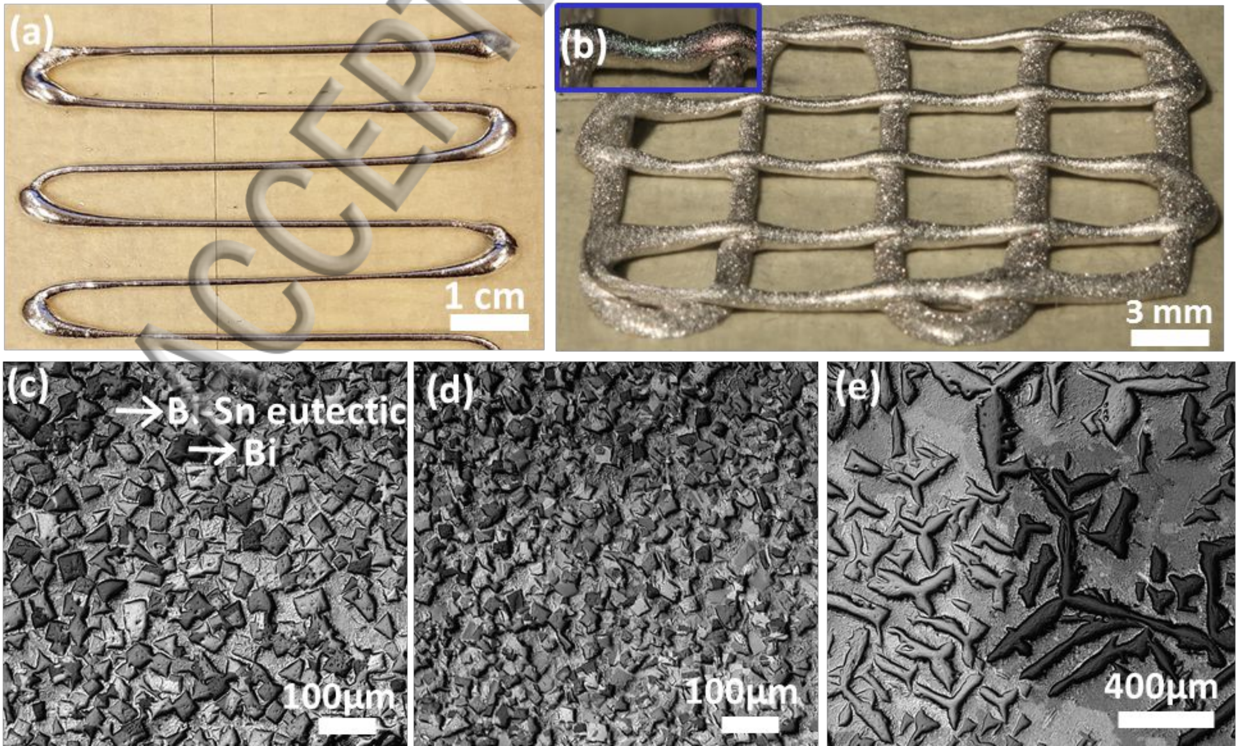
(a)
1 cm
(b)
3 mm
(c)
Sn eutectic
Bi
100µm
(d)
100µm
(e)
400µm

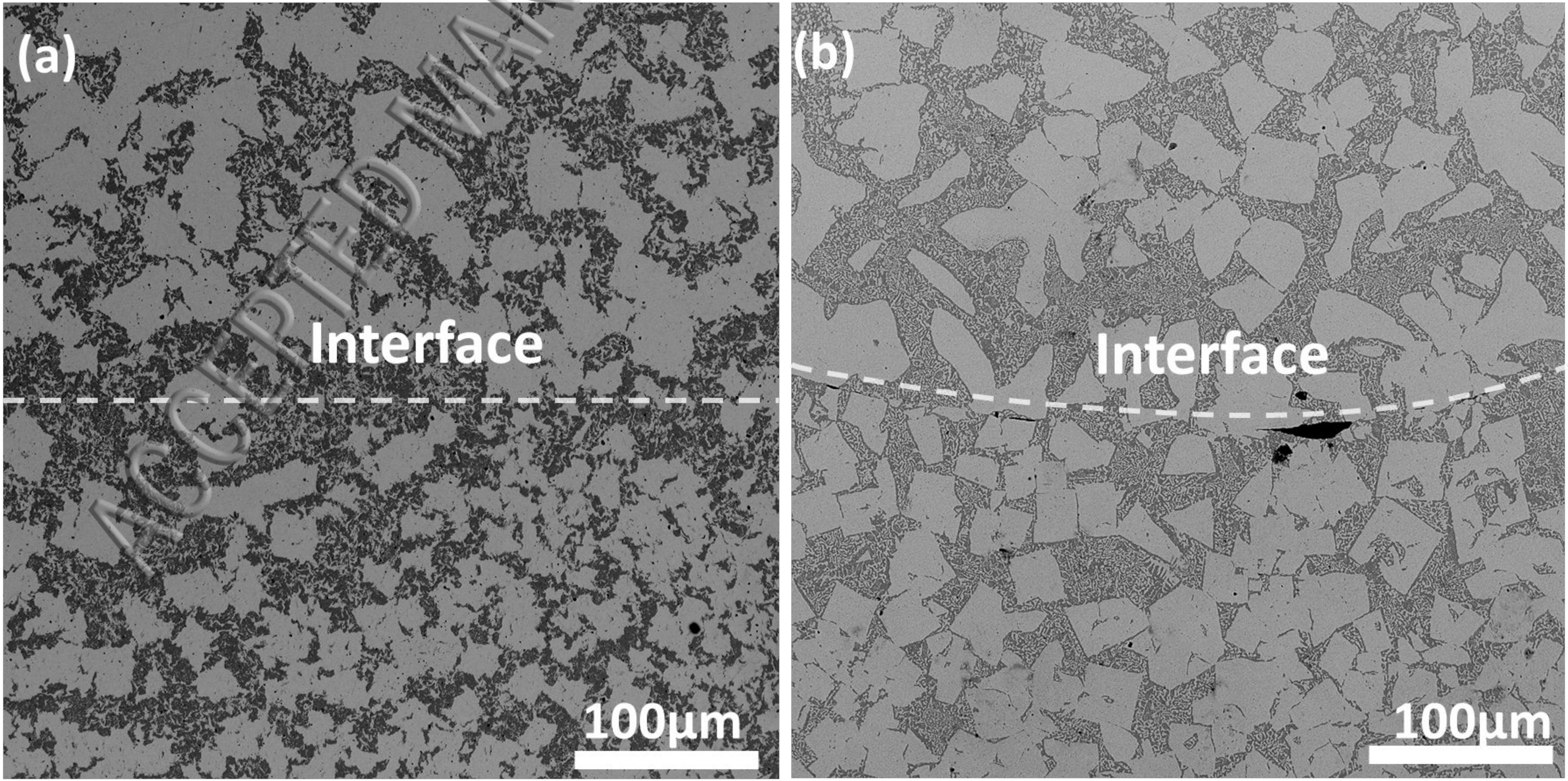

(a)
Interface
100µm
(b)
Interface
100µm